LAWRENCE
LIVERMORE
NATIONAL
LABORATORY

UCRL-CONF-227700

Characterization of Niobium Oxide Films Deposited by High Target Utilization Sputter Sources

R. Chow, A. D. Ellis, G. E. Loomis, S. I. Rana

February 2, 2007

International Conference on Metallurgical Coatings and Thin Films (ICMCTF)
San Diego, CA, United States
April 23, 2007 through April 27, 2007

Characterization of Niobium Oxide Films Deposited by High Target Utilization Sputter Sources

1. INTRODUCTION

High quality, refractory metal, oxide coatings are required in a variety of applications such as laser optics [1], micro-electronic insulating layers [2], nano-device structures [3], electro-optic multilayers [4], sensors [5] and corrosion barriers [6]. A common oxide deposition technique is reactive sputtering because the kinetic mechanism vaporizes almost any solid material in vacuum. Also, the sputtered molecules have higher energies than those generated from thermal evaporation, and so the condensates are smoother and denser than those from thermally-evaporated films. In the typical sputtering system, target erosion is a factor that drives machine availability. In some situations such as nano-layered capacitors, where the device's performance characteristics depends on thick layers, target life becomes a limiting factor on the maximizing device functionality [7]. The keen interest to increase target utilization in sputtering has been addressed in a variety of ways such as target geometry [8], rotating magnets [9], and/or shaped magnet arrays [10]. Also, a recent sputtering system has been developed that generates a high density plasma, directs the plasma beam towards the target in a uniform fashion, and erodes the target in a uniform fashion [11]. The purpose of this paper is to characterize and compare niobia films deposited by two types of high target utilization sputtering sources, a rotating magnetron and a high density plasma source.

The oxide of interest in this study is niobia because of its high refractive index. The quality of the niobia films were characterized spectroscopically in optical transmission, ellipsometrically, and chemical stoichiometry with X-ray photo-electron spectroscopy. The refractive index, extinction coefficients, Cauchy constants were derived from the ellipsometric modeling. The mechanical properties of coating density and stress are also determined.

2. EXPERIMENTAL DETAILS

Two sputtering sources were used in this study: a 125 mm diameter sputter source with a rotating magnet array [12]; and a high density plasma (HDP) source with a 150 mm diameter orifice [13]. High target utilization with the rotating magnet array is achieved by spinning the plasma over the target face, thereby increasing the area where target erosion occurs. The rotating magnetron (RM) used in this study had the magnet array drive by an air motor spinning at 480 rpm. In the high density plasma system, the plasma diffuses out of the orifice, and two electromagnets sustain and guide the plasma beam towards the target. The target, uniformly bathed with the plasma, is sputtered upon application of a negative potential. The target diameter in the HDP experiments was 10 cm. Details of the operation of the high density plasma source is previously described [11,14].

Each sputtering source was installed in its respective stainless steel vacuum chamber. Figures 1a and b are sketches of the chambers. Both had cryo- and turbo- pumps. The substrates holders did not have a means of temperature control. Deposition runs were

made at pressures of 3.3 mPa or lower. The Nb targets were 99.95% pure. Substrates were glass slides and Si(100)-doped wafers, unless noted otherwise. Kapton sheets were used in the HDP source coatings to determine the thin film stress.

Other deposition parameters in the RM process were a throw distance of 21 cm, deposition power of 2 to 3.2 kW, Ar gas flow of 77 sccm. The oxygen flow was controlled by a dual-wavelength plasma emission monitor (PEM) [15]. The dual-optical fiber system collected and transmitted the plasma intensities of the Ar^+ and Nb^+ to the PEM controller. The controller had an algorithm to ratio the intensities together in order to smooth out the plasma oscillations caused by the rotating magnet array. The PEM would maintain an oxygen flow that kept the plasma emission ratio at a fraction of the baseline ratio obtained without any oxygen flowing. In other words, the lower the PEM set-point value, the higher the oxygen flow into the chamber. Thicknesses of the RM-deposited coatings for spectrophotometric, ellipsometric, and XPS analysis were 100 to 300 nm thick. Table I list the thicknesses according to the plasma emission set-points. Stress measurements at the 10% and 25% set-points were determined from 2.0 and 4.0 micron, respectively, thick oxides deposited on Si(100) wafers.

Other deposition parameters in the HDP process were a throw distance of 12 cm, deposition power on the target of 1.7 kW, Ar and O_2 flow of 140 sccm and 60 sccm, respectively. The plasma was inductively generated with a 4kW RF power supply and the orifice electromagnet set to 340 gauss, as measured at the center of the plasma source opening (the electromagnet power supply at 148 A for this magnetic filed strength). The

target electromagnet was set to a field strength that would confine and guide the plasma beam onto the target. Sputtering is initiated when a negative potential was applied to the target, which was 1 kV in this study. HDP deposited coatings were 100 nm thick for ellipsometric and XPS analysis and 320 nm thick for the spectrophotometry measurements. The deposition rate of the Nb oxide with these HDP source parameters were 1.0 to 1.4 nm/s.

The transmittance of the Nb oxide films were performed from 800 to 300 nm using a Cary 5000 UV-VIS-nIR spectrophotometer. The spectral contributions of the glass slides were accounted for by calibrating the spectrophotometer background noise with an uncoated glass slide inserted in the beam path. The coated glass substrates were then measured in transmittance to reveal the spectral effects of the coating.

Variable angle spectroscopic ellipsometry was performed using a Woollam V-VASE® HS-190 ellipsometer system. The angles used were 65°, 70° and 75°. The wavelengths used in this spectroscopy were from 193 nm to 1770 nm. A Nb oxide / native Si oxide / Si substrate stack was the initial layer definition in the analysis application, using the optical properties of the silicon single crystal and its native oxide that were supplied with the analysis application. In the visible wavelength regime, a Cauchy and Urbach formalisms were used to derive the complex refractive index as a function of wavelength in the visible regime. In the short wavelength regime, a Tauc-Lorentz oscillator model, suitable for amorphous materials, was used to fit the ellipsometry data for the extinction coefficients and then the Kramers-Kronig relationship was used to derive the refractive

indices [16]. On the visibly absorbing coatings, the layered model was changed to one with graded optical properties, allowing a better fit to the ellipsometric data.

The XPS analysis was obtained after sputter etch of about 200 A with Ar^+. This step was intended to remove surface contaminants that may interfere with the chemical analysis,

3. RESULTS AND DISCUSSION

Figure 2 is the reactive sputtering hysteresis curve plotting the normalized plasma intensities as a function of oxygen flow. The RM was powered at 2 kW, the Ar flow was 77, and the oxygen mass flow controller in flow control mode. The hysteresis curve was obtained by incrementally increasing the oxygen flow to and from the oxidic target condition. The decrease in the plasma intensity, a result of decreasing deposition rate, was recorded per oxygen flow setting. At around 27 sccm of oxygen flow, the target would fully oxidized with seconds. By using the PEM system, plasma intensities below 35% could be sustained without completely poisoning the target. In the range between 35% to 10% of the "zero oxygen flow" plasma intensities, Nb oxides could be produced that were transparent to absorbing oxides. Figure 2 annotates these observations within the graph.

Figure 3 has the spectrophotometer scans of the Nb oxides deposited from both the rotating magnetron (RM) and HDP sources. Three samples from the RM depositions show quantitatively the decreasing absorption with decreasing set-point on the PEM. The transmittance scan of the coatings deposited at the 10% set-point and from the HDP

source are transparent down to a wavelength of about 400 nm. The exact wavelength cannot be determined from these scans because of the constructive interference between multiple orders of quarter wave optical thicknesses creating the transmittance minima and maxima in the UV wavelengths. There is also some variation of the UV wavelength cut-off. This may be attributed to changes to the bandgap of the coated materials. But it is more likely caused by impurity and thickness variations of the glass slides. The oxide coating deposited at the moderate flow of 20% set-point did not visually appear absorbing. However, in the transmittance scan, this sample is more absorbing than the oxides deposited by both the HDPS and at the highest PEM oxygen flow setting of 10%.

Figure 4 has the dispersion curves of the complex refractive indices as determined from ellipsometry. This data shows that the extinction coefficient behavior are identical for the transparent oxides, which is measurably detectable at wavelengths less than 340 nm, a definitive UV cut-off wavelength compared to the spectrophotometric data of the previous figure. The real parts of the dispersion curves of the transparent oxides show some variation in magnitude which may be caused by density or chemical variations. The RM-deposited oxide from the highest oxygen flow (10% set-point) has a dispersion curve lower than that from the moderate oxygen flow (25% set-point). This may be caused by excessive incorporation of oxygen vapor and a decrease in film density. Another explanation could be that the oxide at moderate flow is more metal-rich than the oxide deposited with a higher oxygen flow. The extinction coefficients, k at 350 nm, are 0.0021, 0.0093, and 0.041 for the oxides deposited oxygen flows at the 10%, 25%, and 30% set-points, respectively. The dispersion curve is given from the magnetron

deposited oxide at a low oxygen flow (35% set-point) which produced an absorbing oxide. The extinction coefficient is about 0.10 from 600 nm to 1770 nm wavelength regime. The refractive index is about 2.2 in the same wavelength range. The Cauchy constants, for wavelength in micron units, is listed in Table 1 for the transparent oxides, deposited by the HDPS and the RM with similar oxygen flows.

Figure 5 is the comparison of the Nb oxides deposited from this study and with those from other reactively-sputtered Nb oxides. The oxide films deposited at the high oxygen flow has similar dispersive behavior as those films deposited by DC magnetron reactive-sputtering [17]. The refractive index at 633 nm is close to that of an IBS deposited Nb oxide [18]. The films deposited by ref. 19 are also reactive DC magnetron deposited but have a lower dispersion curve. They determined the density of their films from X-ray reflectometry measurements to be 87% of bulk Nb_2O_5. From their optical measurements, one can determine a bulk refractive index of 2.4 at λ = 633 nm for Nb_2O_5. The packing density of the oxide films can be determined from the Clausius-Mossotti relationship,

$$P = (n_f^2-1)\,(n_b^2+2) / (n_f^2+2) / (n_b^2-1), \qquad \text{Eqn. [1]}$$

and are listed in Table I for the non- and slightly absorbing oxide films, assuming the Nb_2O_5 phase. The films deposited in this study appear to have at least the same or higher packing densities than other reactively sputtered deposited films [17-19].

Figure 6 is the high resolution XPS scans of the Nb oxide films on Si substrates. The curves were adjusted for surface charging based on the energy shift from the C 1s peak. The Nb_2O_5 phase is represented by the Nb 3d5/2 and 3d3/2 doublet observed near 207.5 eV and 210.0 eV, respectively. The NbO phase is represented by the Nb 3d5/2 and 3d3/2 doublet near 207.5 eV and 203.8 eV, respectively [20]. The mixed Nb oxide phase was observed on both the oxides RM-deposited on the Si and glass samples. The RM coatings, even at the highest oxygen flow, showed a mixture of the pent- and monoxide phases. The HDP coating only shows the pentoxide phase. The XPS data also gives the atomic concentrations of the metal and oxygen. Table II lists the O:Nb atomic ratio as a function of PEM set-point and from the HDP coating. The trend is that as the set-point increase, corresponding to a decrease in oxygen flow, the oxygen concentration decreases in the coating. On the other hand, the HDP coating is at the stoichiometric ratio of 2.5 or greater, indicating an adequate, if not excessive, concentration of oxygen was available during this process.

From the atomic concentrations and the chemical formulas of the Nb mon- and pentoxides, we can determine that the magnetron deposited oxide at the highest oxygen flow is about 58% of the Nb_2O_5 phase. What is difficult to reconcile is the presence of the NbO phase in the RM depositions, especially at the highest oxygen flow. Ref. [21] noted that whenever the presence of sub-oxides was detected, the color of the coating was gray or reflecting. Granted that they always detected NbO along with with NbO_2. However, NbO has a lower O:Nb ratio than NbO_2, and would have more of a metallic appearance.

There are two possible mechanisms where NbO can be generated in the rotating magnetron configuration. One mechanism is an insufficient oxygen concentration at the surface of the substrate. Another is sputtering of a sub-oxide from the rotary magnetron target. As the plasma sweeps around the target, the monoxide forms on the freshly sputtered Nb target area before the plasma completes one revolution, and the plasma sputters this oxide onto the substrate. The observation, though, that in spite of the monoxide presence, the oxide film at the high oxygen flow is still transparent as measured spectrophotometrically and by ellipsometry.

The film stress of the oxide coatings are compressive except for the oxide coating deposited at a low oxygen flow with the rotating magnetron. Table II lists the film stresses in the last column. The stress for the HPD-deposited oxide was calculated from a 320 nm thick coating on Kapton® sheet. This compressive stress is higher than that deposited at elevated substrate temperatures by reactive DC sputtering [17] but comparable to those deposited by IBS [18]. The stresses from the RM coatings were calculated from microns thick oxide coatings on Si wafers, and are close to stress-free oxide states. The small variation in stress that makes the coating switch from compressive to tensile may be caused by vapor incorporation in the coatings such as water [17] or process gasses [22].

4. SUMMARY

Niobium oxide coatings deposited from sources that utilize the target efficiently have been characterized. Optical, chemical, and mechanical properties have been provided. A PEM was required to control the oxygen flow to deposit transparent Nb oxide in the RM system. In the HDP source process, a high oxygen flow was used to deposit transparent oxides. The UV cut-off wavelength starts at $\lambda < 340$ nm for the transparent Nb oxide coatings.

Visibly transparent films on the order of 200 nm thick is not an indicator of the Nb oxide phases composition within the film. The Nb oxide deposited with the HDP source has only the Nb_2O_5 phase. The oxides from the RM source consisted of the Nb_2O_5 and NbO phases, even in films deposited at the maximum oxygen flow setting.

Future work in this project would be to decrease concentration of NbO in the magnetron coatings. One test would be to deposit Nb oxide without rotating the magnet array. Another would be to increase the oxygen concentration at the substrate plane in the magnetron sputtering system. This might be achieved by moving the PEM to position that collects more of the Nb emission signal and then flow at higher oxygen rates. The chamber configuration near the substrate could be changed to increase the containment of the oxygen vapor in the substrate area. Another approach would be to activate the oxidation reaction at the surface of the substrate through an ion assist.

ACKNOWLEDGEMENTS

Appreciation is extended to Ron Synowicki of J.A.Woollam for ellipsometric analysis.

This work was performed under the auspices of the U.S. Department of Energy by University of California, Lawrence Livermore National Laboratory under Contract W-7405-Eng-48.

REFERENCES

1. M. R. Kozlowski, R. Chow, I. M. Thomas, "Optical coatings for high power lasers," chap. in *Handbook of Laser Science and Technology*, ed. M. J. Weber, CRC Press, Inc., Boca Raton, 767-812, 1995.

2. S.J. Kim, B.J. Cho, M.B. Yu, M.F. Li, Y.Z. Xiong, C. Zhu, Chin A., D.L. Kwong, IEEE Electron Device Letters, 26 (2005) 625-7.

3. F. Richter, H. Kuper, P. Schlott, T. Gessner, C. Kaufmann, Thin Solid Films, 389 (2001), 278-83.

4. Z.W. Fu, J.J. Kong, Q.Z. Qin, J Electrochem. Soc., 146 (1999) 3914-18.

5. S. Murray, M. Trudeau, D.M. Antonelli, Advanced Materials, 12 (2000) 1339-42.

6. N. Hara, E. Takahashi, J.H. Yoon, and K. Sugimoto, J Electrochem. Soc., 141 (1994) 1669-74.

7. D. Bach, H. Stormer, R. Schneider, D. Gerthsen, J. Verbeeck, 12 (2006), 416-423.

8. L. Lamont, Jr., US Patent No. 4457825, 3 July 1984.

9. C.B. Garrett, US Patent No. 4444643, 24 Apr. 1984.

10. R.E. Demarray, J.C. Helmer, R.L. Anderson, Y.H. Park, R.R. Cochran, V.E. Hoffman, Jr., US Patent No. 5252194, 12 Oct. 1993.

11. P.J. Hockley, M.J. Thwaites, G. Dion, "High density plasma deposition," SVC 48th annual technical conference proceedings, Society of Vacuum Coaters, 2005.

12. Gencoa Ltd, Full-face erosion circular magnetron, United Kingdom.

13. Plasma Quest, Ltd., Plasma launch system, United Kingdom.

14. R. Chow, M.A. Schmidt, A.W. Coombs, J. Anguita, M.J. Thwaites, "Nb Oxide Film Deposition Using a High-Density Plasma Source," SVC 49th annual technical conference proceedings, Society of Vacuum Coaters, 2006.

15. Gencoa Ltd, Speedflo plasma emission monitoring system , United Kingdom.

16. J.A. Woollam Co., Inc., *Guide to using WASE32™* , WexTech, New York, 269, 1995.

17. H. Kupfer, T. Flügel, F. Richter, P. Schlott, Surface and Coatings Technol., 116-119 (1999) 116-120.

18. C.C. Lee, C.L. Tien, J.C. Hsu, Appl. Optics, 41 (2002), 2043-7.

19. S. Venkataraj, R. Drese, O. Kappertz, R. Jayavel, M. Wuttig, Phys. Stat. Sol. A, 188 (2001) 1047-58.

20. J.F. Moulder, W.F. Stickles, P.E. Sobol, K.D. Bomben, *Handbook of X-ray Photoelectron Spectroscopy*, Eds. J. Chastin and R.C. King Jr., Physical Electronics, Inc., Eden Prairie, MN, 1995, p. 11.

21. C.L. Lee and C.R. Aita, J Appl. Phys., 70 (1991) 2094-2103.

22. H. Leplan, B. Geene, J.Y. Robic, Y. Pauleau, J of Appl. Physics, 78 (1995) 962-8.

Table I Oxide thicknesses and deposition rates from rotary magnetron coatings.

PEM set-point	Film Thickness (nm)	Deposition Rate (nm/s)
10%	104	0.44
25%	293	0.88
30%	296	1.35
35%	222	1.28

Table II Chemical, optical and mechanical properties of Nb oxide films that were deposited from the two sputtering systems for high target utilization. HDP = high density plasma source; P = Nb pentoxide, M = Nb monoxide

Process Variation	Oxide Phase	O/Nb Atomic Ratio	Cauchy Constants for λ = 0.40 to 1.70 μm			Refractive Index	Packing Density	Film Stress
			A	B	C	n @ 633 nm	n_{bulk} = 2.4	MPa
HDPS	P	2.5 to 3.9	2.217	0.0701	-0.0058	2.35	98%	-517
10%	P, M	1.67	2.156	0.0578	-0.0055	2.25	94%	-6.1
25%	P, M	1.63	2.211	0.0375	-	2.31	96%	-18.1
30%	P, M	1.59	2.133	0.117	-0.0283	2.22	93%	11.2

FIGURE CAPTIONS

1. (a) Vacuum chamber for depositions using the rotary magnetron. Chamber is 100 cm in diameter x 50 cm deep. (b) Vacuum chamber for the depositions using the high density plasma source. The rotating magnetron is located at Gun #1 position. LCW = low conductivity water.

2. Reactive sputtering hysteresis curve using manual and a plasma emission monitor to establish oxygen flows for transparent Nb oxide coatings. Manual oxygen flows are (♦) symbols. Flows controlled by the plasma emission monitor (PEM) are (◊) symbols.

3. Spectrophotometric transmission scans of Nb oxides on glass slides with depositions at various PEM set-points and with the HDP source. As the set-point decreases, indicating higher oxygen flow rates, the Nb oxides become more transparent. The oxide deposited with the HDP source is transparent.

4. Complex refractive indices of oxide films deposited on Si(100) wafers. Films were deposited at various PEM set-points and with the HDP source.

5. Refractive index comparisons with other sputter deposited Nb oxide films. (—) HDP source; (**---**) RM at PEM 25% set-point; (---) RM at PEM 10% set-point; (—) DC magnetron 17; (**▬**) DC magnetron [19]; (▲) Ion beam sputtered [22]; (●) bulk refractive index derived from ref. 19.

6. High resolution X-ray photospectroscopy of the Nb 3d electron. The doublet at 207.5 eV and 210.0 eV is indicative of the Nb pentoxide phase. The doublet at 207.5 eV and 203.8 eV is indicative of the Nb monoxide phase.

7. The O:Nb atomic ratio for the oxide coatings deposited at various plasma emission monitor set-points and with the high density plasma (HDP) source. The HDP concentrations are plotted at the 15% point for reference only. Concentrations were provided by the XPS scans.

Fig 1a

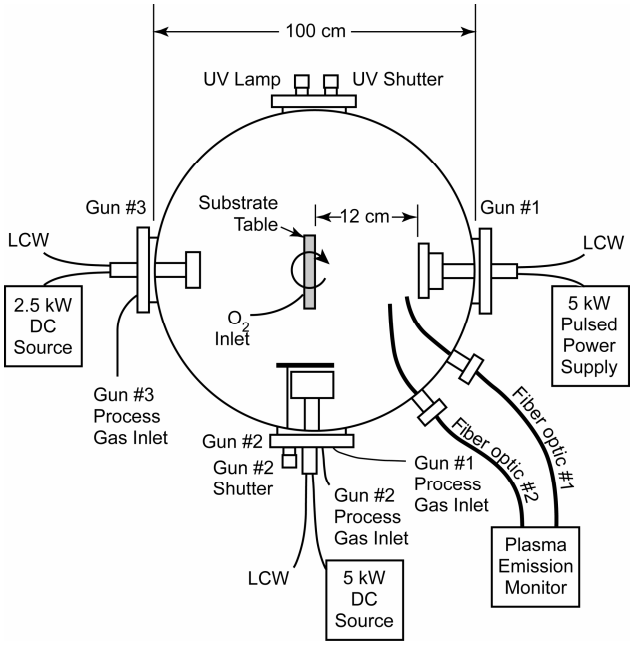
100 cm
UV Lamp
UV Shutter
Gun #3
Substrate Table
12 cm
Gun #1
LCW
LCW
2.5 kW DC Source
O_2 Inlet
5 kW Pulsed Power Supply
Gun #3 Process Gas Inlet
Fiber optic #1
Fiber optic #2
Gun #2
Gun #2 Shutter
Gun #1 Process Gas Inlet
Gun #2 Process Gas Inlet
Plasma Emission Monitor
LCW
5 kW DC Source

Fig1b

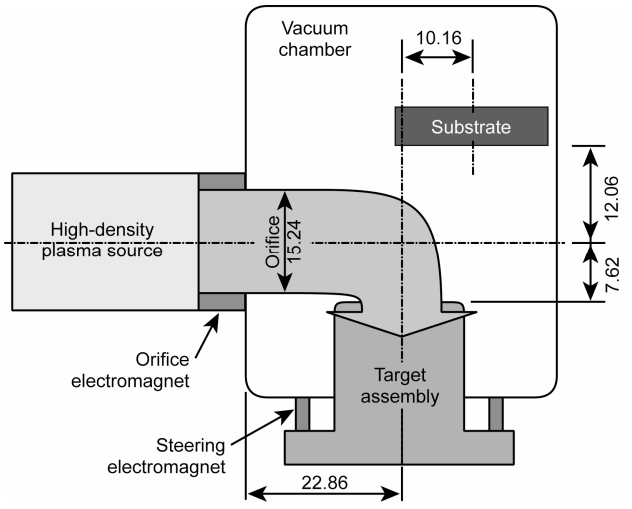
Vacuum chamber
10.16
Substrate
12.06
High-density plasma source
Orifice 15.24
7.62
Orifice electromagnet
Target assembly
Steering electromagnet
22.86

Fig 2

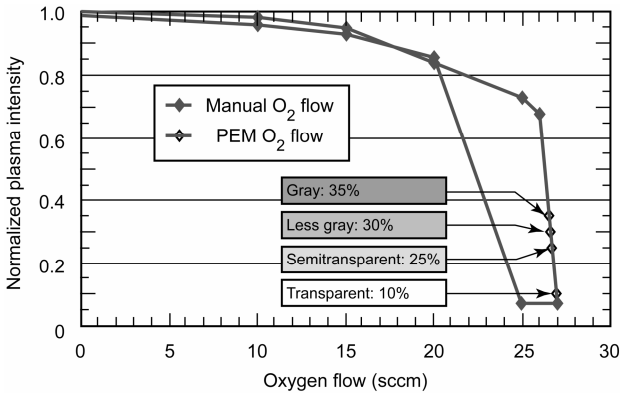

Fig3

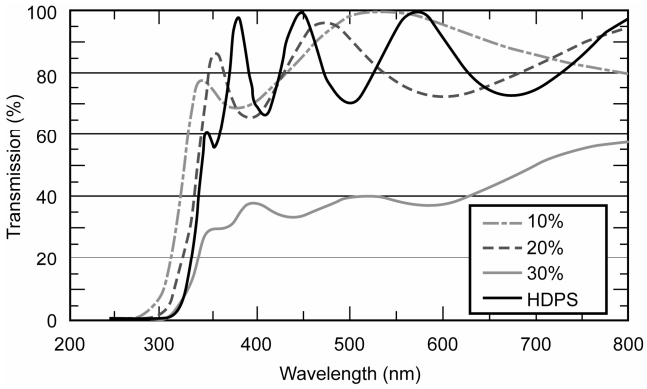

Fig4

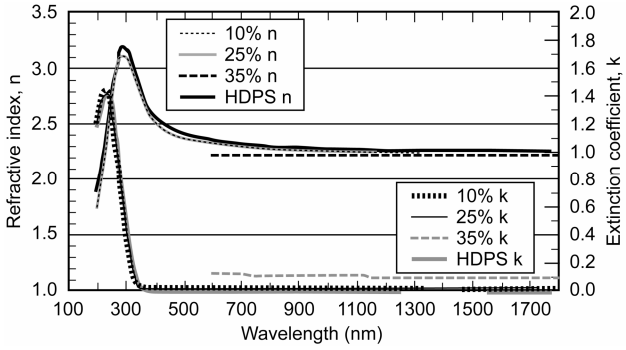

Fig5

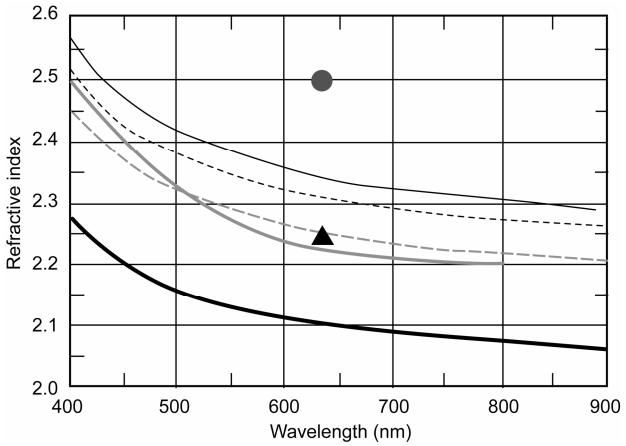
Refractive index
2.6
2.5
2.4
2.3
2.2
2.1
2.0
400
500
600
700
800
900
Wavelength (nm)

Fig6

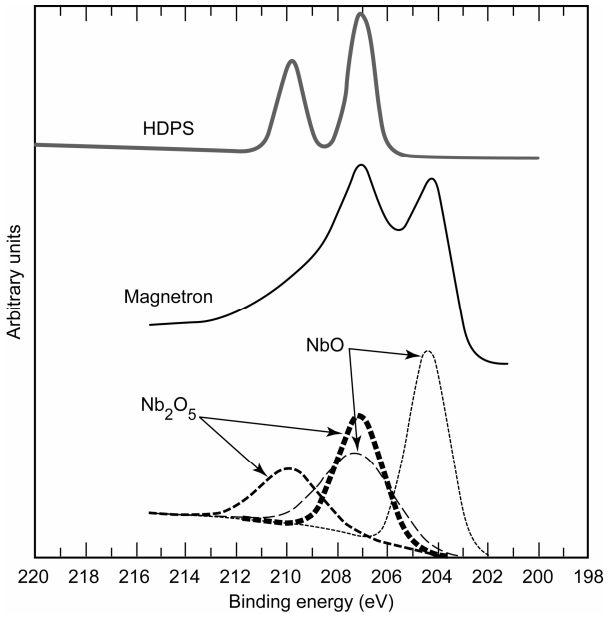
HDPS
Magnetron
NbO
Nb2O5
Arbitrary units
220
218
216
214
212
210
208
206
204
202
200
198
Binding energy (eV)